IEEE Access
Multidisciplinary | Rapid Review | Open Access Journal

Received September 4, 2019, accepted September 13, 2019, date of publication September 17, 2019,
date of current version September 30, 2019.

Digital Object Identifier 10.1109/ACCESS.2019.2941923

Smart Pleural Effusion Drainage Monitoring System Establishment for Rapid Effusion Volume Estimation and Safety Confirmation

PI-YUN CHEN[1], CHIA-HUNG LIN[1,2], CHUNG-DANN KAN[3,4], NENG-SHENG PAI[1], WEI-LING CHEN[5,6], AND CHIH-HSIEN LI[1]

[1]Department of Electrical Engineering, National Chin-Yi University of Technology, Taichung 41170, Taiwan
[2]Artificial Intelligence Application Research Center, National Chin-Yi University of Technology, Taichung 41170, Taiwan
[3]Department of Surgery, National Cheng Kung University Hospital, Tainan 70101, Taiwan
[4]College of Medicine, National Cheng Kung University, Tainan 70101, Taiwan
[5]KSVGH Originals and Enterprises, Kaohsiung Veterans General Hospital, Kaohsiung 81362, Taiwan
[6]Department of Engineering and Maintenance, Kaohsiung Veterans General Hospital, Kaohsiung 81362, Taiwan

Corresponding authors: Neng-Sheng Pai (pai@ncut.edu.tw) and Chia-Hung Lin (eechl53@gmail.com)

This work was supported by the Ministry of Science and Technology, Taiwan, under Contract MOST 107-2221-E-006-156-MY2 and Contract MOST 108-2221-E-167-005-MY2.

ABSTRACT Pleural effusion is the pathologic accumulation of body fluids around the unilateral or bilateral lungs that is primarily caused by heart disease. A chest radiograph is a rapid examination technique used to provide a preliminary diagnosis of lung and heart diseases. Computer-aided diagnosis with the digitalized image is an automated approach that addresses the drawbacks of manual inspection. In this study, two corner detectors along with a two-dimensional convolution process are used to enhance the chest X-ray image for an accurate extrapolation of the bilateral lung cavities. Based on bounding box pixel analysis, the pixel ratios of the lung anatomy between normal and abnormal conditions can be estimated to identify the pleural effusion size. Next, a smart drainage monitoring system is developed to improve the current functions of the traditional drainage tool and confirm the drainage safety, including (a) drainage volume and required time detection, (b) unplanned removal warning, and (c) physiological status monitoring. The experimental result will be used to determine the feasibility of the proposed effusion volume estimation algorithm and the efficiency of the smart drainage monitoring prototyping tool. The proposed smart drainage monitoring system and the computer-aided method with digitalized images can be further applied in real clinical practice in the intensive care unit.

INDEX TERMS Pleural effusion, corner detector, bounding box pixel analysis, smart drainage monitoring system.

I. INTRODUCTION

Peural effusion is the pathologic symptom of the accumulation of body fluids in the chest cavity surrounding the lungs and can be divided into several types as follows: edema and hemothorax (exudates and exuded), chylothorax, and biliothorax. This abnormal condition is caused by heart disease, pneumonia, pulmonary hypertension, pleuropulmonary malignancy, trauma, and chest surgery (open heart surgery) [1]–[3]. Among these diseases, pleural effusion is generally caused by heart diseases or chest surgery, and pleural drainage is the most commonly performed procedure in the intensive care unit (ICU) after vascular catheterization and tracheal intubation. It has been reported that 41% of patients admitted to the ICU have pleural effusion [4], [5]. When the effusion volume is in excess of 1,000–1,500 mL, this pathologic condition will affect breathing by limiting the lung expansion, resulting in interference with atelectasis, dyspnea, and arrhythmias [6], [7]. Pleural effusion can be detected during physical examinations using a stethoscope and imaged examinations using chest ultrasound, chest computed tomography (CT) scan, and upright chest X-ray techniques [6]–[10]. CT is considered as the gold standard, but it is expensive and not easy to perform on ICU patients. Pleural effusion can be easily detected by a chest ultrasound to visualize effusion and to distinguish between different types with the best sensitivity

The associate editor coordinating the review of this manuscript and approving it for publication was Okyay Kaynak.

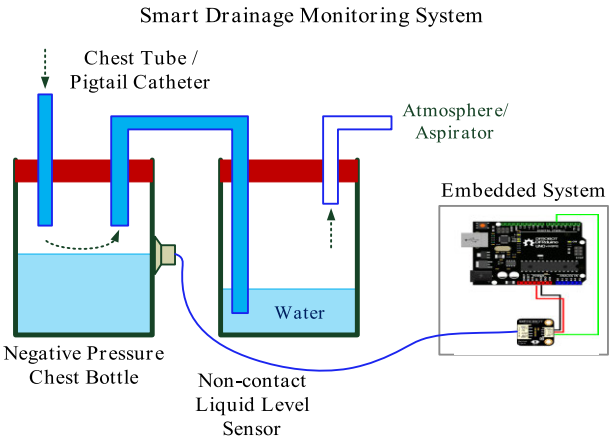

FIGURE 1. Negative pressure chest bottle and smart drainage monitoring system.

and specificity. Plain chest X-ray has long been the reference examination for lung images, and it is possible only in the anterior–posterior manner in the ICU [11]. When clinical examination suggests pleural effusion sizes, pleural drainage will be performed via a catheter (chest tube or pigtail catheter) inserted through the thoracic wall to a negative pressure chest bottle. Before pleural effusion drainage, estimation of the adequate drainage volume is required to prevent the occurrence of reexpansion pulmonary edema (RPE) [12], [13].

In clinical procedure, after estimations of the pleural effusion volume and site, the principle of negative pressure will be applied to drain the pleural effusion into the chest bottle, as seen in Figure 1. However, current drainage devices and techniques are not equipped with automatic warning sensors for monitoring, such as the following: (1) no warning function when the target drainage volume is achieved; (2) a warning function when drainage did not achieve an desired duration, which might indicate that there is obstruction in the drainage catheter; (3) no heart rate monitoring during drainage; and (4) a function to monitor unplanned removal of drainage catheters (self-removal or accidental removal) in patients during drainage. In view of the above statements, it is necessary to establish an assistive method to rapidly estimate the effusion volume for further fluid drainage. In addition, we also intend to establish a smart drainage monitoring system for monitoring physiological signals, drainage volume, and safety confirmation during the pleural drainage treatment.

In visualization examination, inspection of a digitized medical image is a straightforward approach used by clinicians to rapidly diagnose lung abnormalities. A chest X-ray image reveals pleural effusions as black portions in air spaces, as shown in Figure 2(a). In chest X-ray image examination, posteroanterior and lateral image views can show the fluid volume within the pleural space. As shown in the right-hand side in the X-ray image, under normal condition, an obvious sharp angle (red circle) is present at the lower thoracic cavity. The bilateral thoracic cavity can hold 2,000–3,000 mL in volume [14], [15]. During the occurrence of pleural effusion, the chest X-ray method can provide estimates of small, moderate, and severe effusion sizes. CT scans can construct the chest inside and outside image and provide more detailed images of many types of tissue, such as lungs, bones, and blood vessels. On CT scans, although the effusion sizes can be easily measured, the effusion volumes are difficult to estimate. The possible effusion volume must be quantified via linear regression analysis with dimension parameters (effusion heights and depths) and application software and is dependent on clinician experiences [16]. An ultrasound probe can also create images of the inside of the thoracic cavity to locate the position of the effusion. Hence, clinicians can further obtain a fluid sample for analysis and determine the location to insert a catheter into the thoracic cavity between the patient's ribs. The abovementioned imaging examinations provide promising results for estimating the effusion size. However, the patient's position has a significant impact on the estimation of pleural effusion volume, with a high mean prediction error. An adequate estimation of the effusion volume is a major challenge due to certain reasons such as thoracic cavity area determi- nation, diaphragm position, and diaphragmatic hernia [17]. Hence, a plain chest X-ray can be used to directly categorize the effusion sizes or the abnormal conditions through anteroposterior and lateral views, such as lung diseases or pleural effusion. However, there is a lack of an automatic method to estimate the pleural effusion volume. Pattern recognition is performed using manual inspection and has some limitations, such as the following: (1) although it can identify the effusion sizes, it cannot estimate the effusion volumes; (2) poor-quality X-ray images must be enhanced to visualize the lung contour using the image enhancement method; (3) the diagnostic results depend on the radiologists' interpretations and experiences, and (4) much time is required to perform the inspections. Hence, the computer-aided method with digitalized medical images is proposed to automatically bind the highlighted area on the chest X-ray images so that clinicians can pay more attention to these specific areas (bounding box) in real clinical practice, such as pleural effusion and pneumonia [18].

For an automated screening method, computer-aided examination can rapidly identify the desired object region by preanalyzing medical images. Firstly, the image enhancement process is employed to modify the gray- scale values and readjust the image contrast using nonlinear intensity transformation functions, such as gradation function, histogram equalization, Fourier filtering, and convolution process [19]–[23]. Next, the contour algorithm and object localization algorithm [24], [25] use the modified gray gradient information to identify the boundaries of the desired objects within an image. As a result, the desired objects (subimages) can be extracted and further applied to pattern recognition or classification application. Hence, both image enhancement and segmentation processes are important for feature extraction in automatic digital image processes. However, traditional intensity transformation functions are sensitive to noise and cannot easily detect the boundary in

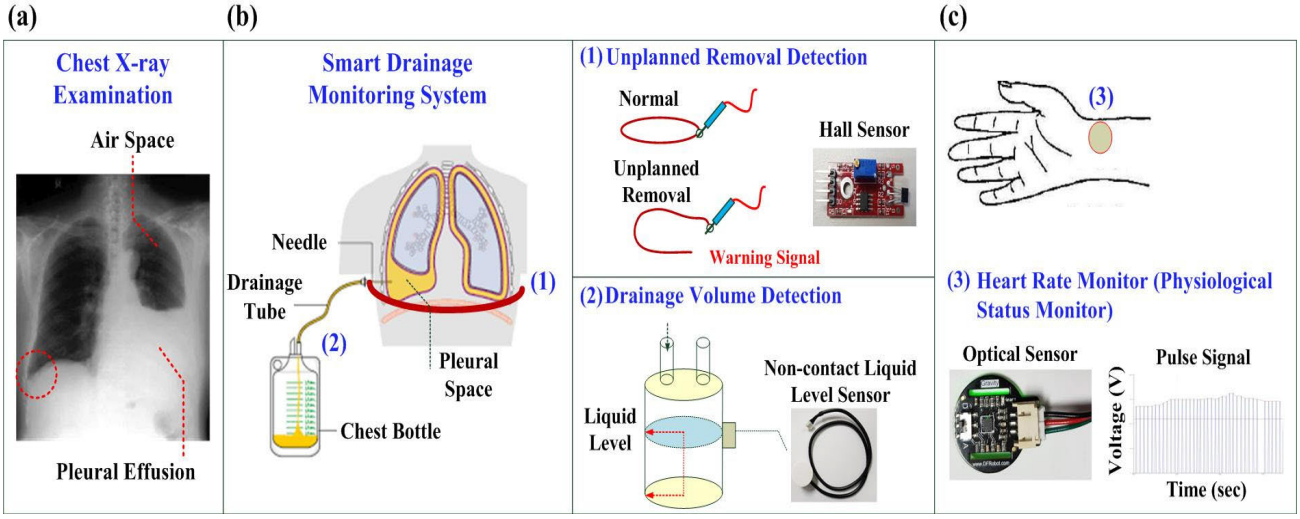

FIGURE 2. Digitized medical image examination and functions of smart drainage monitoring system. (a) Chest X-ray image, (b) Unplanned removal and drainage volume detection using Hall sensor and non-contact liquid level sensor, (c) Heart rate monitor using optical sensor.

poor-quality images, such as a Sobel operator or a Laplacian operator. In this study, a Harris corner detector [26]–[29] is applied for image enhancement and segmentation applications. A corner detector is also a convolution process method. The method involves performing a local operation with a 2×2 mask matrix to transform intensity into a feature map through sliding the mask window over the image. In this study, two- dimensional (2D) image processing involving two Harris mask matrices (horizontal and vertical masks) are applied based on Gaussian windows to enhance the bilateral lung contours. Based on the shape of the bilateral lung contours, bounding box pixel analysis, as an automated inspection method, is employed to estimate the effusion volumes according to the following ranges: small effusion size ($<$ 500 mL), moderate effusion size (500-1,000 mL), and large effusion size ($>$1,000 mL). Through experimental tests, we will demonstrate the feasibility of the automated 2D digital image process to enhance lung contours, resulting in the desired subimages used to estimate the effusion volumes.

Furthermore, as shown in Figure 2(b), the principle of negative pressure is used to drain the effusion in the body to a pair of chest bottles, as it is important to be used for pneumothorax. In the ICU, physiological status can be continuously monitored using an optical sensor during drainage treatment, such as heart rhythms, blood pressures, and saline replenishment. These parameters are available on the monitor in the ICU. However, there is no sensor available that can automatically monitor the drainage volume and rate and provide warning information when the drainage tubes are removed. According to the annual data of the Taiwan Patient Safety Reporting System, drainage catheter abnormalities account for 5% of hospital tubing events in Taiwan. These abnormalities include tubing dislodgment, obstruction, and misconnections, among which dislodgment events are classified as self-removal and accidental detachment, the so-called unplanned tubing removal. Approximately 70% of these events are unplanned tubing removal events that often occur because of physiological and depressive symptoms in the patients. Rapid drainage or a large drainage volume may cause cardiac load and lead to bilateral RPE symptom [12], [13]. In order to prevent the above abnormalities, a smart drainage monitoring system must be used during drainage, as shown in Figures 2(b) and 2(c). When any abnormality occurs during drainage, a warning notification can be sent to the nurses. The smart drainage monitoring system developed in this study includes the following: (1) drainage volume and speed estimation; (2) physiological status monitoring; and (3) safety confirmation. We integrate the Hall sensor, liquid-level sensor, and optical sensor to implement the smart drainage monitoring system's warning functions regarding drainage volume, heart rate, and safety confirmation.

The remainder of this article is organized as follows: Section II describes the methodology, including the Harris corner detector, drainage volume estimation, and smart drainage monitoring system implementation. Sections III and IV presents the experimental results and conclusions.

II. METHODOLOGY

A. HARRIS CORNER DETECTOR

A corner in an image is a point whose local neighborhood stands in two dominant or different edge directions. These corners are regions in the image with large variation in intensity in all directions. These corners also contain the most important feature or information that can be used to minimize the amount of processed data for motion tracking, image stitching, building mosaics, stereo vision, and image representations in computer vision applications. The Harris

corner detector [21]–[24] is a rapid method to identify the differences in intensity for a displacement of $(\Delta x, \Delta y)$ in all directions in an image. Given a 2-dimensional (2D) image, the sum of squared differences between (x, y) and $(x + \Delta x, y + \Delta y)$ can be expressed as

$$E(x, y) = \sum_{(x,y)\in w(x,y)} [I(x + \Delta x, y + \Delta y) - I(x, y)]^2 \quad (1)$$

Shifted Intensity : $I(x + \Delta x, y + \Delta y)$ is the shifted intensity at the sliding window$(x + \Delta x, y + \Delta y)$

Intensity : $I(x, y)$ is the intensity at pixel (x, y)

where $w(x, y)$ is the sliding window and can be defined as a rectangular window or a Gaussian window that gives weights to the pixels underneath. Let I_x and I_y be the partial derivatives of I, $I(x + \Delta x, y + \Delta y)$ can be approximated by Taylor expansion as

$$I(x + \Delta x, y + \Delta y) \approx I(x, y) + I_x(x, y)\Delta x + I_y(x, y)\Delta y \quad (2)$$

Thus, equation (1) can be modified as

$$E(x, y) \approx \sum_{(x,y)\in w(x,y)} [I_x(x, y)\Delta x + I_y(x, y)\Delta y]^2 \quad (3)$$

Equation (3) can also be expressed in matrix form:

$$E(x, y) \approx (\Delta x, \Delta y) M \begin{pmatrix} \Delta x \\ \Delta y \end{pmatrix}, \quad (4)$$

$$M = \sum_{(x,y)\in w(x,y)} \begin{bmatrix} I_x^2 & I_x I_y \\ I_x I_y & I_x^2 \end{bmatrix} \quad (5)$$

where I_x and I_y are the gradients at pixel (x, y); matrix M is the structure tensor of a pixel, which is a characterization of information of all pixels within the sliding window. Equation (4) can be written as

$$E(x, y) = AI_x^2 + CI_x I_y + BI_y^2 = [\Delta x\ \Delta y] \begin{bmatrix} A & C \\ C & B \end{bmatrix} \begin{bmatrix} \Delta x \\ \Delta y \end{bmatrix}, \quad (6)$$

$$A = I_x^2 \otimes w, \quad B = I_y^2 \otimes w, \ C = I_x I_y \otimes w \quad (7)$$

where we can assign the elements A, B, and C of matrix M to determine if the sliding window corresponds to a corner as follows:

- if $A \approx 0$, $B \approx 0$, and $C = 0$, then the pixel (x, y) has no feature of interest,
- if $A = 0$, B is the large positive value, and $C = 0$, then an edge can be found,
- if A and B are the large positive values and $C = 0$, then a corner can be found.

According to equation (5), the structure tensor M is a covariance matrix of gradients for pixels around the pixel investigated within the sliding window. For corners, the distribution ranges of derivatives I_x and I_y are large. Hence, the corner is characterized by a large variation of $E(x, y)$ in all directions of the vector (x, y). By analyzing the eigenvalues of M, matrix M should have two large positive values for an interest point, as satisfying A and B are the large positive values $(A = B)$ and $C = 0$. Eigenvalues measure the variances of interest points along the eigenvectors. To avoid computing the eigenvalues (computational expensive), in this study, an enhancement mask as a sliding window can be implemented using a 2×2 mask matrix, which can be defined as a Gaussian window,

$$M = \begin{bmatrix} A & C \\ C & B \end{bmatrix} = \begin{bmatrix} e^{\frac{-\lambda_1}{\sigma}} & 0 \\ 0 & e^{\frac{-\lambda_2}{\sigma}} \end{bmatrix} \quad (8)$$

where λ_1 and λ_2 are the eigenvalues, and σ is a scaling parameter for tuning the elements A and B. At the pixel location (x, y), if both eigenvalues are large, then this location is at a corner; one large and one small eigenvalue identifies a step edge; and two small eigenvalues identify a low-contrast region.

In the 2D spatial domain, the corner detector by convolving both horizontal and vertical directions can be expressed as

1) HORIZONTAL DIRECTION

$$G_x s(x, y) = \sum_{i=0}^{1} \sum_{j=0}^{1} M(i, j) s(x + i, y + j) \quad (9)$$

2) VERTICAL DIRECTION

$$G_y s(x, y) = \sum_{j=0}^{1} \sum_{i=0}^{1} M(j, i) s(x + j, y + i) \quad (10)$$

where $M(i, j) = M(j, i)$ is the element in the mask matrix;

$s(x, y)$ is the gray-scale value at pixel (x, y), s $\in [0, 255]$; $x = 1, 2, 3, \ldots, p$ and $y = 1, 2, 3, \ldots, q$ are the image width and height, respectively. The gray gradient can be defined as

$$\nabla s(x, y) = G_x s(x, y) + jG_y s(x, y) \quad (11)$$

$$|\nabla s(x, y)| = \sqrt{(G_x)^2 + (G_y)^2} \approx |G_x| + |G_y|, \quad |\nabla s| = \frac{|G_x| + |G_y|}{255} \quad (12)$$

Using the G_x and G_y, we can convolve the original image to obtain the gray gradient. Depending on the variations of the gray-scale value $s(x, y)$, the gray gradient can enhance the visibility of the intensity matter variations (image contrast) using the corner detector $(\lambda_1 = \lambda_2 = 0.5, \sigma = 0.6 - 1.0)$ while convolving both horizontal and vertical directions and can detect the image edge, as shown the moderate and severe effusions in Figures 3(c) and 3(d). After the image enhancement processes, the active contour (snakes) algorithm and the gradient vector flow (GVF) method [24], [25] are generally used to locate the object boundaries in computer vision and image processing applications. The GVF method is computed as a diffusion of gradient vectors of gray-level form an image. Hence, both Harris corner and GVF snake can

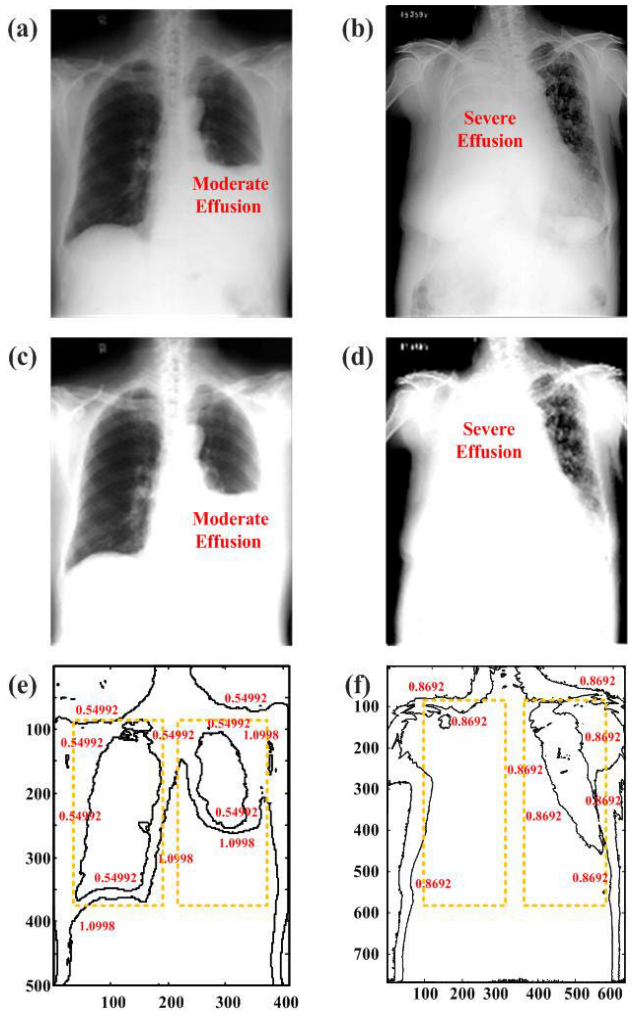

FIGURE 3. Digital image process using the corner detector. (a) and (b) Original images for moderate and severe effusions, (c) and (d) Detected image edge for moderate and severe effusions, (e) and (f) Contour label text for left and right lungs.

be applied to segment the left and right lung regions in a chest X-ray image. Based on the edge-detected gradients, the desired object region of a distinguishable feature can be located in the image, as shown in the right and left lungs in Figures 3(e) and 3(f).

Figures 3(e) and 3(f) show the isolines of normalized gray gradients for the right and left contour regions in a 2D image. The values of the contour levels can be determined based on the minimum and maximum gray gradients. For example, the minimum values of the contour levels are 0.5499 and 0.8692 to interpret the bilateral lung regions (two subimages) for moderate and severe effusions analysis, as highlighted by the yellow dotted line. For the threshold values, θ_R and θ_L, the numbers of minimum values of the right and left regions are computed via bounding box pixel analysis as

$$\begin{cases} sum_R = sum(\nabla s_R(x,y)) for \nabla s_R(x,y) < \theta_R \times 1.1 \\ sum_L = sum(\nabla s_L(x,y)) for \nabla s_L(x,y) < \theta_L \times 1.1 \end{cases} \quad (13)$$

where $\nabla s_R(x, y)$ and $\nabla s_L(x, y)$ are the gray gradients within the right and left lung regions, respectively, $sum_R(\cdot)$ and $sum_L(\cdot)$ are accumulators to count the pixel numbers of the minimum gradients, and $\theta_R \times 1.1$ and $\theta_L \times 1.1$ are the threshold values for right and left lung regions, respectively. Thus, the pixel numbers of minimum gradients can be rapidly counted within the bilateral bounding right and left lung regions.

B. DRAINAGE VOLUME QANTIFICATION

According to the bounding regions, the total lung capacity (TLC) for the bilateral lungs, $TLC_{R,est}$ and $TLC_{L,est}$, can be estimated as

$$TLC_{R,est} = \frac{TLC_R sum_R}{sum_{R,nor}} \quad (14)$$

$$TLC_{L,est} = \frac{TLC_L sum_L}{sum_{L,nor}} \quad (15)$$

where TLC_R and TLC_L are the bilateral TLCs under normal conditions, and $sum_{R,nor}$ and $sum_{L,nor}$ are the pixel numbers of the minimum gradient under normal conditions. These two indexes, $sum_{R,nor}$ and $sum_{L,nor}$, were the total of the pixel numbers of the minimum gradients, which were counted from the right and left lung regions, where $sum_{L,nor} \approx sum_{R,nor}$-$sum_{Heart}$; sum_{Heart} is the total of the pixel number of the heart-occupied regions. The mean of the pixel number was obtained from healthy subjects (at least 20 male adults and 20 female adults, respectively). TLC is the maximum amount of air that can fill the right and left lungs and can be set as $TLC \approx 6{,}000$ mL [14], [30]. The average lung volumes in healthy female and male adults are 5,800 and 4,200 mL [14], respectively. Hence, we can estimate the fluid-filled volume that accumulates in the chest cavity; the fluid-filled volume of a single chest cavity is approximately 2,800 and 2,100 mL in female and male adults, respectively. The pleural effusion volume (PEV) can be estimated as

- female adult:

$$PEV_R \approx 2100 - TLC_{R,est}(\text{mL}) \quad (16)$$

$$PEV_L \approx 2100 - TLC_{L,est}(\text{mL}) \quad (17)$$

- male adult:

$$PEV_R \approx 2800 - TLC_{R,est}(\text{mL}) \quad (18)$$

$$PEV_L \approx 2800 - TLC_{L,est}(\text{mL}) \quad (19)$$

Hence, the sizes of the chest cavity can be quantified to estimate the fluid-filled volumes and can be divided into three levels of small, moderate, and large effusion sizes as follows:

- small effusion size: approximately 20% of the fluid-filled volume corresponding to < 500 mL;
- moderate effusion size: approximately 20%_50% of the fluid-filled volume, corresponding to 500–1,000 mL;
- large effusion size: approximately $> 50\%$ of the fluid-filled volume, corresponding to $> 1{,}000$ mL.

The decision support system is implemented in a computer-assisted application program for PEV estimation, as shown in Figure 4. The image enhancement, image contour, and drainage volume estimation algorithms can be established

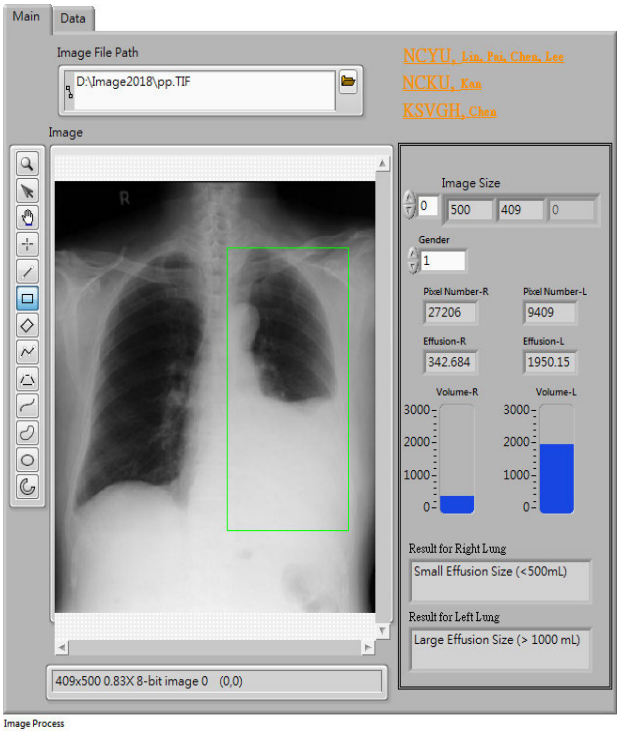

FIGURE 4. Decision support system for drainage volume estimation.

FIGURE 5. Implementation of the smart drainage monitoring system. (a) Detection of unplanned tubing removal, (b) monitoring the heart rate (physiological signal), and (c) estimation of effusion volume.

using the high-level graphical and text- based programming language in LabVIEW programming software (NI^{TM}, Austin, TX, USA) and MATLAB workspace (1994-2019, The MathWorks, Inc. USA). Usually, at most, 1,500 to 2,000 mL can be drained from one side; however, this is also dependent on the patient's condition. After the possible effusion volume is estimated, approximately 800 mL of pleural effusion will be drained each time; this volume may increase to 1,000 mL as the number of sessions increases.

C. SMART DRAINAGE MONITORING SYSTEM IMPLEMENT

As shown in Figure 5, the smart drainage monitoring system is implemented to automatically monitor the drainage effusion volume and physiological signal and also provide warning information when the drainage catheters or tubes are removed by patients themselves. In order to prevent the unplanned tube / catheter removal in patients, a chest-belt warning sensor with Hall detector is designed to be worn on the patient's chest, as shown in Figure 5(a). When the drainage needle is removed by the individual, a warning notification can be sent to the nursing staff. As shown in Figure 5(b), an optical sensor integrating red light source and light receiver [31], [32] is designed as a wristband to be worn on the wrist that is employed to monitor pulse signals (seen in Figure 2(c)) and then calculate the heart rate. The heart rate is estimated every 10 seconds on average, which can be used to monitor sudden life-threatening events, such as RPE during drainage.

With regards to the automatic monitoring of the drainage volume and the drainage speed, the bottoms of these chest bottles are designed in the form of regular shapes, such as circles, squares, or rectangles. This study uses a circular base container as an example for calculation of the desired liquid height, H (cm), of the drainage volume sensor:

$$V_{drained} = A_V H, \quad H = \frac{V_{drained}}{A_V}, \tag{20}$$

$$A_V = \begin{cases} Circle\ Area = \pi r_1^2 \\ Quadrangle\ Area = LW \end{cases} \tag{21}$$

where $V_{drained}$ is the effusion volume (mL) to be drained and can be estimated using equations (16) and (17) for a female adult and (18) and (19) for a male adult. The radius of the circle is r_1(cm); the L(cm) and W(cm) are the length and width of square / rectangular bases, respectively; and H is the height of the liquid-level sensor, as shown in Figure 5(c). In this study, a noncontact liquid-level sensor is employed to detect the desired liquid height. This technique uses the principle of changes in the coupling capacitance distribution and does not require contact with the liquid to sense the liquid height in the chest bottle. The noncontact method will not be affected by pus, blood, and debris in the drainage liquid and has high accuracy. In addition, we can also estimate the required time t (min) for achieving the drainage volume based on the flow rate Q (mL/min):

$$Qt = A_V H, \quad t = \frac{A_V H}{Q} = \frac{V_{drained}}{Q} \tag{22}$$

where Q is the flow rate, which can be measured by a digital flowmeter. As shown in Figure 5(c), this function can monitor the desired drainage volume, $V_{drained}$, and thereby estimate the time requirement, t, for drainage possible to be completed. When drainage exceeds the expected duration, this situation indicates the drainage tubing may be obstructed. In practice, the nursing staff must perform manual inspections periodically check the patients' physiological status, including heart rhythms, blood pressures, or respiratory rates. Our smart drainage monitoring system enables to evaluate the specified time requirement to achieve the pre-set height and determine if drainage is exceedingly fast or slow and can be combined with heart rate monitoring and be used to remind nursing staff to perform transfusion (fluid / blood) during drainage.

The smart drainage monitoring system was implemented in the Arduino®prototyping platform (Uno, Atmel 8-bit CMOS microcontroller 32K bytes self-programmable mechanism, 6 analog inputs, 14 digital inputs / outputs, DI / DO). The platform integrated detection signals from multiple warning sensors and could be used to acquire analog signals to perform 10-bit analog-to-digital conversion at the maximum acquisition rate of 10,000 times/s. The detection algorithms were designed by the C / C++ programming language in the Arduino®circuit board (as seen Figure 11 in Appendix). Therefore, in clinical applications, when any monitored value reached a specified threshold value, such as the desired liquid height, H, the drained time requirement, t, the occurrence of power interruption at the belt sensor, and heart rate abnormalities, a warning signal could directly trigger the light-emitting diode (LED, warning light) and buzzer (alarm) to provide a warning message, thereby alerting the nursing staff to implement the appropriate treatment as soon as possible.

III. EXPERIMENTAL RESULTS AND DISCUSSION

A. PLEURAL EFFUSION VOLUME ESTIMATION

The proposed image preprocessing algorithms were designed on a tablet PC using LabVIEW programming software (NI^{TM}, USA), as displayed in the graphical user interface shown in Figure 4. The anterior–posterior chest X-ray images were collected from the NIH chest X-ray database (NIH Clinical Center) [33]. This NIH database was available in the following DICOM (digital imaging and communication in a medicine format) store hierarchy in Cloud Healthcare API (application programming interface). The chest X-ray images were converted from DICOM format into a tagged image file (TIF) format. The TIF format is a lossless image, the processing of which could take less computation time for routine examinations. Each digital X-ray image was specified in a 409 (image width) × 500 (image length) pixel-sized image, 8 bites/pixel, with 0–255 gray-scale values. In 2D convolution processes, the Harris corner detector and fractional-order enhancement mask were used to perform a local operation to enhance the images. With the appropriate parameters, the 2D convolution operations could highlight the bilateral lung structures, as shown in Figures 6(a) and 6(b). Image enhancement in Figure 6(a) was obtained using the Harris corner detector with eigenvalues, $\lambda_1 = \lambda_2 = 0.5$, and scaling parameters, $\sigma \leq 0.2$ and 0.2 – 0.9. As shown in Figure 6(b), digital image enhancement was obtained using the fractional-order parameters, 0.10 – 0.95. The fractional-order enhancement mask [21], [22] could be constructed on the 4 symmetric directions with three coefficients, 1, $(-v)$, and $(-v)(-v+1)/2$, as described (Figure 10) in the Appendix. The parameters of the Harris corner detector and the fractional-order mask could not fit all X-ray images. Obviously, appropriate scaling parameters, $\sigma = 0.6 - 1.0$, and fractional-order parameters, $v = 0.70 - 0.99$ (parameter v subject to $0 < v < 1$ [21], [22], [34]), were used to assign the mask elements in this study. The image enhancement processes improved the visibility of gradient intensity for further segmentation of the right and left lung cavity structures.

Next, the contour search and object localization algorithms [24], [25] applied the gray gradient changes to determine the boundaries of the bilateral lung contours, as shown in Figure 3. As indicated by the green bounding box in Figure 4, we could obtain the right and left individual images via the bounding box as a 190 (width) × 350 (length) object region. Hence, the minimum gray gradient $\theta_R = \theta_L = 0.5499$ could be determined as the threshold value to count the pixel numbers of the minimum gray gradients using equation (13) within the right and left lung cavity regions. For the case study shown in Figure 6, using the 2D convolution operations, an average threshold value of 0.60 (threshold value $\approx \theta_R \times 1.1 = \theta_L \times 1.1$) was used to separate the minimum gray gradients from the higher gradients in the bilateral bounding box regions, as shown in the blue and green regions in Figures 7(a) and 7(b), respectively, where the blue region indicating the gray gradients was less than the threshold value (0.60); otherwise, the gray gradients were greater than the threshold value for the green region. Therefore, the pleural effusion could be quantified by bounding box pixel analysis using equations (14) and (15), and then the effusion volumes could also be estimated using equations (16)–(19) for female adult and male adult patients. The experimental results with corner convolution and fractional-order convolution are shown in Figure 8(a) and 8(b), respectively.

The experimental results indicated the enhanced image to be similar and stable from the fractional-order parameters, $v = 0.80$ to 0.99, using the fractional-order convolutions. The left and right lung effusion volumes were in the ranges of 1,810.2 – 1,817.6 mL and 490.6 – 501.8 mL, respectively. Using the Harris corner convolutions with scaling parameters, $\sigma = 0.6 - 0.7$, the experimental results showed left and right lung effusion volumes in the ranges of 1575.6 – 1748.5 mL and 70.8 – 409.0 mL, respectively. The large effusion size at the left lung cavity could be identified for a case study. In contrast to fractional-order convolution [34], Harris corner convolution also allowed us to rapidly estimate the effusion volumes and took an average CPU time of 1.1544 s to

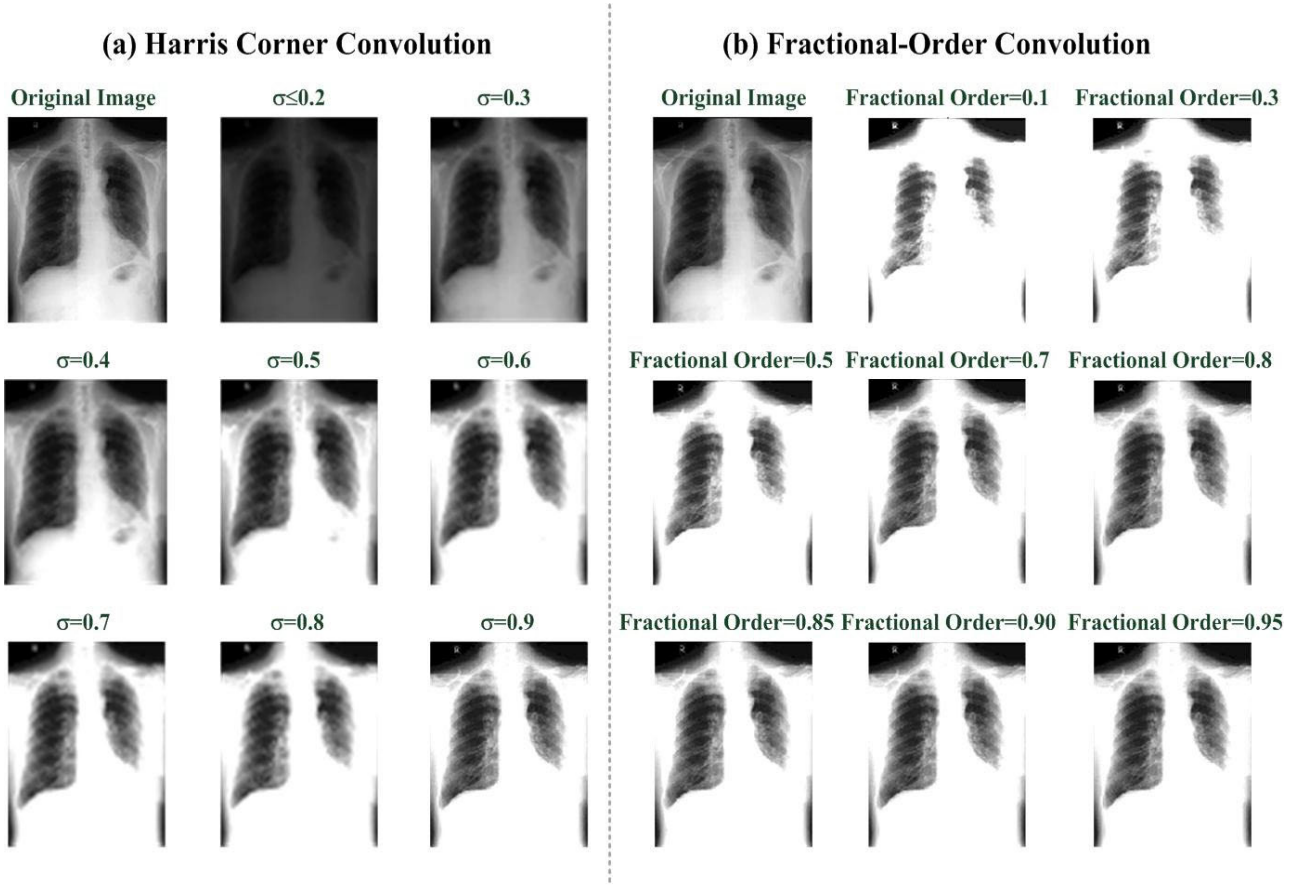

FIGURE 6. Results of image enhancement processes using the 2D convolution processes. (a) Image enhancement using a Harris corner detector (eigenvalues: $\lambda_1 = \lambda_2 = 0.5$, scaling parameters: $\sigma \leq 0.2$–0.9); (b) image enhancement using fractional-order masks (fractional-order parameter = 0.10–0.95).

complete the decision-making process. In addition, to fit all chest X-ray images, the Harris corner detector with eigenvalues, $\lambda_1 = \lambda_2 = 0.5$, and scaling parameter $\sigma = 0.7$ was assigned for all experiments in this study. Satisfying $A = B$ with the appropriate large positive values and $C = 0$, the corner detector could easily detect the differences in intensities (gray gradients) to find the boundaries of desired objects within an image. Next, the contour algorithm was employed to search discontinuities and to indicate the isolines for image segmentation, data extraction, and bounding box pixel analysis in specific areas. In addition, the corner detector was used to easily assign the parameters of the enhancement mask and the fractional-order mask. Therefore, 2D corner convolution also is able to provide promising results in image enhancement and estimating the PEV.

B. SMART DRAINAGE MONITORING SYSTEM TESTING

In clinical practice, analyzing chest X-ray images is a common method used to directly observe the anatomical positions, e.g., the height of the intercostal space could be used to estimate the pleural effusion sizes. The adequate drainage volume could be rapidly estimated using our proposed screening method. The proposed smart drainage monitoring system was used to monitor the desired drainage volume, physiological signals, and safety. The entire system could be divided into two subsystems, as summarized below:

- the first subsystem with the chest-belt warning sensor and the optical sensor was used to detect unplanned tubing removal and monitor heart rate, as shown in Figures 5(a) and 5(b),
- the second subsystem could detect the drainage volume and estimate the drainage duration, as shown in Figure 5(c),

The functions and experimental results of these subsystems are described as follows:

- unplanned tubing removal test: Figure 5(a) shows the chest-belt warning sensor, in which a Hall sensor [14] was employed to detect power interruption. During the occurrence of an unplanned tubing removal, the proposed detection algorithm could detect a low voltage and then produce a high-voltage output to drive a buzzer (alarm) and a LED (warning light) to notify nurses for emergency management,
- heart rate monitoring test: in practice, the drainage speed was extremely high, thus exacerbating cardiac load or heart failure. Drainage of large effusion volumes might result in RPE occurrence [12], [13]. If this event is not immediately discovered and processed, then the

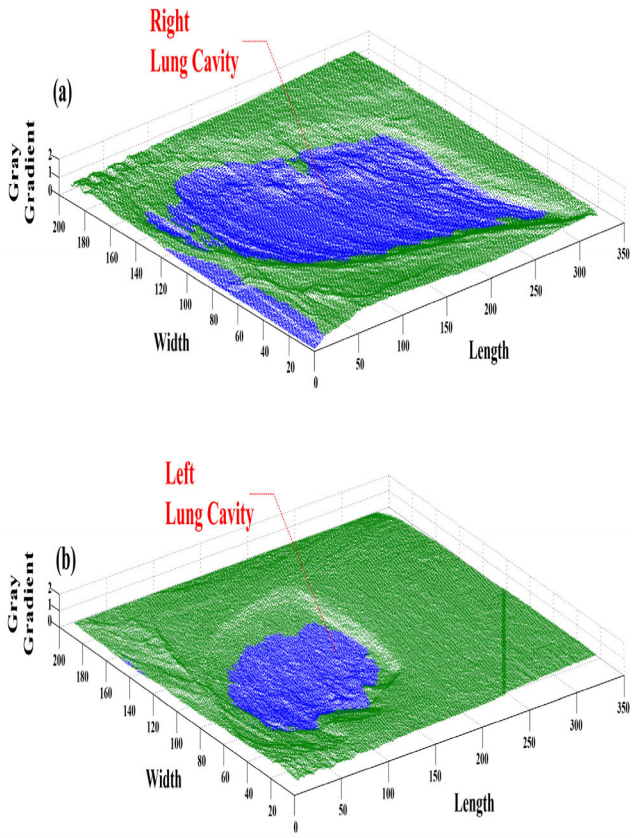

FIGURE 7. Bilateral grey gradient distributions. (a) Grey gradient distributions for the right lung cavity; (b) grey gradient distributions for the left lung cavity.

contralateral lung can be affected, with the resulting complication progressing to bilateral lungs. Hence, monitoring of the heart rate or respiration of patients during drainage is required. As shown in Figure 5(b), an optical sensor with reflecting mode (680 nm red light) was used to detect pulse signals [31], [35]. To validate the feasibility of the optical sensor, a total of seven measurements were made. The average heart rate was 71.58 bpm, as shown in Figure 9,

- effusion volume and duration estimation: assuming that the drained volume was 500 mL after a chest X-ray image examination, the desired volume to be drained could be entered using the keyboard, and then the height of the liquid-level sensor was calculated using equations (20) and (21), for example, the estimated height, $H \approx 6$ cm (radius of bottom circle, $r_1 \approx 5.15$ cm) in Figure 5(c). Next, the noncontact liquid-level sensor (coupling capacitive sensor) was placed at the estimated height H. Using a drainage volume of 500 mL and a flow rate of 20 mL/min in the experimental model, the drainage duration was estimated that a desired drainage volume could be completed in $t \approx 25$ min according to equation (22), as shown in the LCD display in Figure 5(c). This function could monitor whether the drainage was overly fast or slow based on the drainage speed.

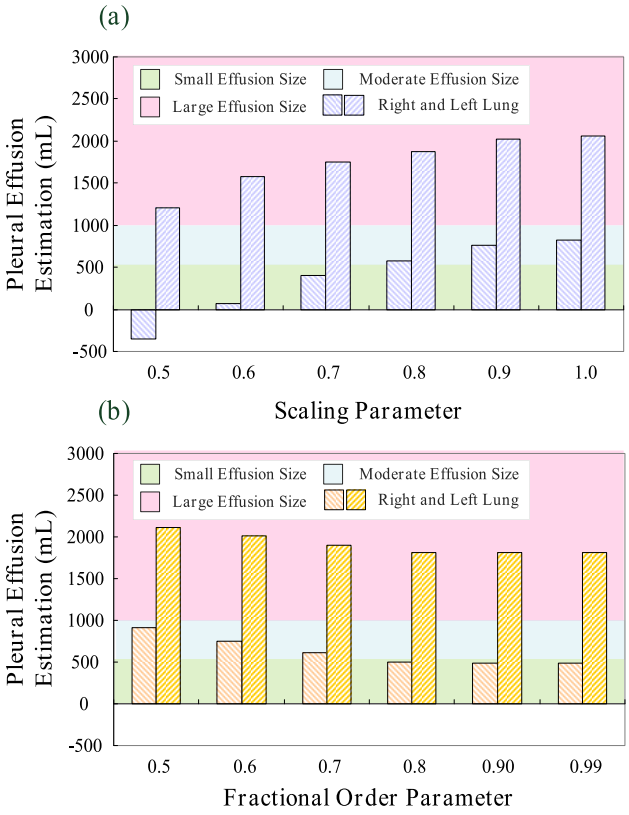

FIGURE 8. The results of pleural effusion estimation. (a) Estimated effusion volumes versus scaling parameters, $\sigma = 0.5$–1.0; (b) estimated effusion volumes versus fractional-order parameters, $v = 0.5$–0.99.

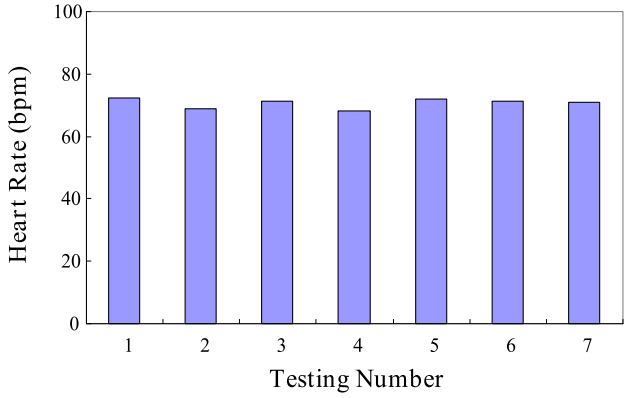

FIGURE 9. Heart rate (bpm) monitoring results.

In general, the drainage volume must not exceed 1,000 mL in each drainage duration, and continuous drainage should not exceed 500 mL/Hr. After the administration of local anesthesia and tube insertion (28- to 32-F chest tubes), the drainage tube was connected to the negative pressure chest bottle. The proposed smart drainage monitoring system has promising attributes, including: (1) the physiological status could be continuously monitored by an optical sensor during the drainage treatment, such as heart rhythms, blood pressures, and saline replenishment, which avoids rapid drainage of large effusion volume that would tend to cause RPE; (2) before drainage, all interfaces should be secured using tape to prevent patients from removing the chest tube on their

own or accidental removal (pulling) events. The proposed chest-belt warning sensor could detect the unplanned and accidental removal events; (3) when the drainage volume reaches a desired liquid height, the liquid-level sensor produces a high-voltage signal to trigger the yellow LED and the buzzer as warning signals to inform nurses; and (4) the drainage volume could be periodically monitored to determine the expected time for completing the task at any time to determine whether the drainage is overly fast or slow. This function could be combined with heart rate monitoring and remind nurses to conduct transfusion (saline or blood) during drainage; in addition, its function could also indicate whether the tube is blocked.

The proposed smart system could improve the traditional drainage system regarding the continuous monitoring physiological status and safety confirmation. The application scope of the proposed smart system could also be extended to monitor drainage in the thoracic cavity and the abdominal cavity (ascites drainage). This smart system has high feasibility and potential commercialization [36]. The entire multi edge sensors, hardware circuitry, and application software could be integrated into an embedded system. In future work, to the following will be performed: 1) assess the sensors and hardware circuitry electrical safety (IEC 60601 series standard [37]) and the biocompatibility of the wearable device, and the healthcare design [38]; 2) verify the relevant safety, stability, and efficacy of the monitoring system, including the detection algorithms and application software; and 3) ensure the system conforms to skin irritation standards to ensure the smart wearable device is suitable for the human body or the medical setting after commercialization.

IV. CONCLUSION

Currently, drainage is a required process in chest surgery, simple chest aspiration/drainage, lung cancer surgery, or other surgeries, among which, simple chest aspiration / drainage accounts for the majority of the cases (55%), and chest surgeries and other surgeries account for 45% of the cases. Approximately fifty thousand people require drainage in Taiwan per year. Approximately thirteen thousand people develop malignant tumors in lung cancer every year in Taiwan, and nine thousand people die of lung cancer. Patients suffering lung cancer with pleural effusion also require drainage. The proposed monitoring system could be used in both pleural and ascites drainage. Hence, the innovative design of the system in this study could fulfill the medical device market demand for drainage systems. In the digital image process, 2D corner detector, contour search, and object localization algorithms were employed to enhance the bilateral lung cavity regions, thereby, enabling location of the specific region for further bounding box pixel analysis. The higher contrast image simplifies determination of a proper threshold value. Depending on the selection of the proper threshold value, the higher contrast image could be used to rapidly segment the desired objects from a digitized image. However, the proposed corner detector was found to be limited in overall lung disease diagnosis because of the lack of a set of finite chest X-ray images for each abnormality and the medical diagnosis being dependent on the radiologists. In this study, applying a 2D corner detector and bounding box pixel analysis was validated as being able to rapidly screen pleural effusion. Two corner detectors with eigenvalues $\lambda_1 = \lambda_2 = 0.5$ and scaling parameter $\sigma = 0.7$ was found to exhibit good performance in image enhancement and segmentation in X-ray image processing. For commercialization in clinical applications, it is required to verify the biocompatibility, electrical safety, and effectiveness (including the hardware, detection algorithms, and application software design), and risk assessment, according to the IEC 60601 series standard. The proposed smart monitoring system can further be implemented through a compact embedded system without limiting the patient's range of motions in clinical applications.

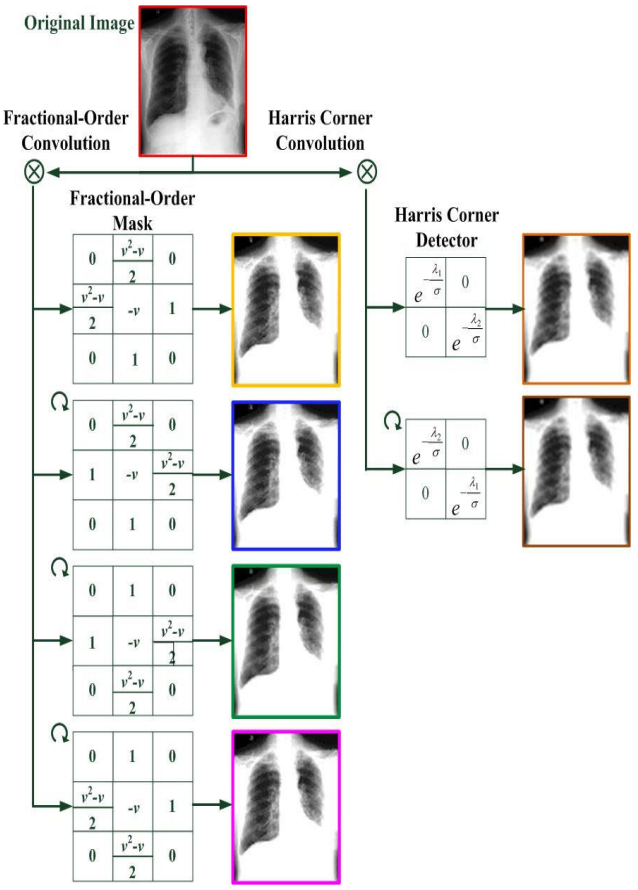

FIGURE 10. Two-dimensional convolution processes with fractional-order masks and a Harris corner detector.

APPENDIX

2D CONVOLUTION PROCESSES WITH ENHANCEMENT MASKS

Figure 10 show the 2D convolution processes with fractional- order masks and a Harris corner detector. The fractional-order masks have rotation capability that are rotated clockwise every 90 degrees (rotation invariant) and mask in four directions. These fractional-order masks are

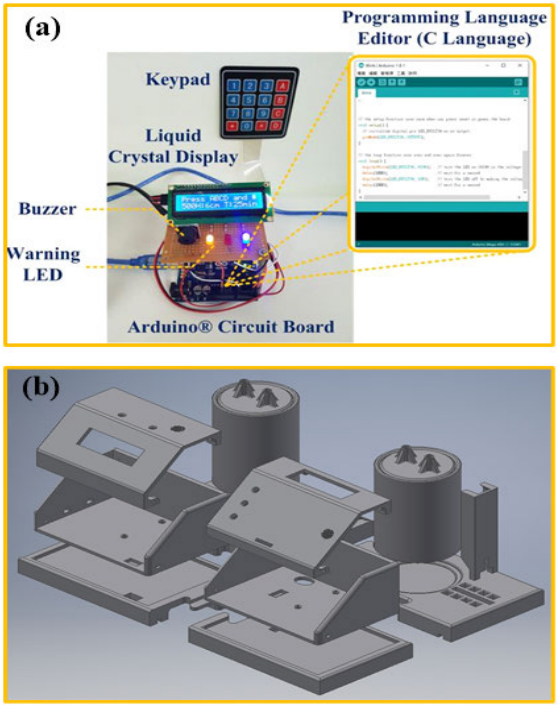

FIGURE 11. Prototyping platform. (a) Arduino®-based monitoring system and programming language editor (b) Implementation of the smart drainage monitoring system with the 3D printing technique.

used to describe the edges present and to remove noise. In contrast to the fractional-order masks, the Harris corner detector is used to reduce image noise and aliasing artifacts through convolution with the structure tensor, M. By adjusting the eigenvalues of M, the characterization of the corner detector can be easily determined for finding an edge ($\lambda_1 \approx 0$ and λ_2 has some large positive value) and a corner (both λ_1 and λ_2 have large positive value) in computer vision applications. Therefore, its method can be accurate in distinguishing between edges and corners. It provides good repeatability with changing rotation and illumination and is used in image database retrieval and matching. In this study, the Harris corner detector with the Gaussian function (using a small standard deviation) was also used to enhance the original image by convolving both horizontal and vertical directions and reduce image noises.

ARDUINO®PROTOTYPING PLATFORM (UNO):

Figure 11(a) shows the Arduino®-based monitoring system and programming language editor (C language). The C programming language editor is used to implement the detection algorithm in a microprocessor. With the multi-end sensors, such as coupling capacitive sensor, optical sensor (red light), and Hall sensor, the proposed monitoring system can continuously monitor the drainage volume, physiological signal, and safety. The 3D printing technique can also be used to design the appearance of the monitoring system, as seen in Figure 11(b), so that the hardware unit can be miniaturized and operation will become simple. In addition, its applications have high feasibility and potential commercialization to extend in both thoracic cavity and abdominal cavity.

REFERENCES

[1] R. W. Light, "Pleural effusions," *Med. Clin.*, vol. 95, no. 6, pp. 1055–1070, 2011.
[2] N. G. Yalcin, C. K. Choong, and N. Eizenberg, "Anatomy and pathophysiology of the pleura and pleural space," *Thoracic Surgery Clin.*, vol. 23, no. 1, pp. 1–10, 2013.
[3] H. Yu, "Management of pleural effusion, empyema, and lung abscess," *Seminars Interventional Radiol.*, vol. 28, no. 1, pp. 75–86, 2011.
[4] L. Vetrugno, G. M. Guadagnin, D. Orso, E. Boero, E. Bignami, and T. Bove, "An easier and safe affair, pleural drainage with ultrasound in critical patient: A technical note," *Crit. Ultrasound J.*, vol. 10, no. 18, pp. 1–10, 2018.
[5] L. Vetrugno, E. Bignami, D. Orso, M. Vargas, G. M. Guadagnin, F. Saglietti, G. Servillo, G. Volpicelli, P. Navalesi, and T. Bove, "Utility of pleural effusion drainage in the ICU: An updated systematic review and META-analysis," *J. Crit. Care*, vol. 52, pp. 22–32, Aug. 2019.
[6] E. Usta, M. Mustafi, and G. Ziemer, "Ultrasound estimation of volume of postoperative pleural effusion in cardiac surgery patients," *Interact. Cardiovascular Thoracic Surgery*, vol. 10, pp. 204–207, Feb. 2010.
[7] M. P. Moy, J. M. Levsky, N. S. Berko, A. Godelman, V. R. Jain, and L. B. Haramati, "A new, simple method for estimating pleural effusion size on CT scans," *Chest*, vol. 143, no. 4, pp. 1054–1059, 2013.
[8] J. Yao, W. Han, and R. M. Summers, "Computer aided evaluation of pleural effusion using chest CT images," in *Proc. IEEE Int. Symp. Biomed. Imag., Nano Macro*, Jun./Jul. 2009, pp. 241–244.
[9] H. M. Zaeim, C. Scheffer, M. Blanckenberg, and K. Dellimore, "Evaluation of the use of frequency response in the diagnosis of pleural effusion on a phantom model of the human lungs," in *Proc. 36th Annu. Int. Conf. IEEE Eng. Med. Biol. Soc.*, Aug. 2014, pp. 3418–3421.
[10] S. A. Rezaeieh and A. M. Abbosh, "Review of systems for the detection and monitoring of accumulated fluids in the human torso," in *Proc. Int. Symp. Antennas Propag.*, Nov. 2015, pp. 1–4.
[11] E. Brogi, L. Gargani, E. Bignami, F. Barbariol, A. Marra, F. Forfori, and L. Vetrugno, "Thoracic ultrasound for pleural effusion in the intensive care unit: A narrative review from diagnosis to treatment," *Crit. Care*, vol. 21, Dec. 2017, Art. no. 325.
[12] R. Kasmani, F. Irani, K. Okoli, and V. Mahajan, "Re-expansion pulmonary edema following thoracentesis," *Proc. CMAJ*, vol. 182, no. 18, pp. 2000–2002, 2010.
[13] N. Taira, T. Kawabata, T. Ichi, T. Yohena, H. Kawasaki, and K. Ishikawa, "An analysis of and new risk factors for reexpansion pulmonary edema following spontaneous pneumothorax," *J. Thoracic Disease*, vol. 6, no. 9, pp. 1187–1192, 2014.
[14] V. S. Patil and M. V. Bhalsing, "A review on functions of Rakt Dhatu and Prana Vayu to establish lung function capacity," *Int. J. Innov. Res. Med. Sci.*, vol. 3, no. 1, pp. 1656–1658, 2018.
[15] K. Sembulingam and P. Sembulingam, *Essentials of Medical Physiology*, 6th ed. New Delhi, India: Jaypee Brothers Medical Publisher, 2012.
[16] M. Hazlinger, F. Ctvrtlik, K. Langova, and M. Herman, "Quantification of pleural effusion on CT by simple measurement," *Biomed Paper Med. Fac. Univ. Palacky Olomouc Czech Republic*, vol. 158, no. 1, pp. 107–111, 2014.
[17] L. Vetrugno, E. Brogi, F. Barbariol, F. Forfori, and E. Bignami, "A message in the bottle," *Anesthesiology*, vol. 128, p. 677, 2017.
[18] I. Sirazitdinov, M. Kholiavchenko, T. Mustafaev, Y. Yixuan, R. Kuleev, and B. Ibragimov, "Deep neural network ensemble for pneumonia localization from a large-scale chest X-ray database," *Comput. Elect. Eng.*, vo. 78, pp. 388–399, Sep. 2019.
[19] R. Manniesing, M. A. Viergever, and W. J. Niessen, "Vessel axis tracking using topology constrained surface evolution," *IEEE Trans. Med. Imag.*, vol. 26, no. 3, pp. 309–316, Mar. 2007.
[20] D. Huang, C. Zhu, Y. Wang, and L. Chen, "HSOG: A novel local image descriptor based on histograms of the second-order gradients," *IEEE Trans. Image Process.*, vol. 23, no. 11, pp. 4680–4695, Nov. 2014.
[21] Y.-F. Pu, J.-L. Zhou, and X. Yuan, "Fractional differential mask: A fractional differential-based approach for multiscale texture enhancement," *IEEE Trans. Image Process.*, vol. 19, no. 2, pp. 491–511, Feb. 2010.
[22] Y. Zhang, Y. Pu, and J. Zhou, "Construction of fractional differential masks based on Riemann–Liouville definition," *J. Comput. Inf. Syst.*, vol. 6, no. 10, pp. 3191–3199, 2010.
[23] J.-L. Chen, C.-H. Huang, Y.-C. Du, and C.-H. Lin, "Combining fractional-order edge detection and chaos synchronisation classifier for fingerprint identification," *IET Image Process.*, vol. 8, no. 6, pp. 354–362, Jun. 2014.

[24] R. Klette, *Concise Computer Vision: An Introduction Into Theory and Algorithms* (Undergraduate Topics in Computer Science). London, U.K.: Springer-Verlag, 2014.
[25] C. Xu and J. L. Prince, "Snakes, shapes, and gradient vector flow," *IEEE Trans. Image Process.*, vol. 7, no. 3, pp. 359–369, Mar. 1998.
[26] F. Mokhtarian and R. Suomela, "Robust image corner detection through curvature scale space," *IEEE Trans. Pattern Anal. Mach. Intell.*, vol. 20, no. 12, pp. 1376–1381, Dec. 1998.
[27] P. I. Rockett, "Performance assessment of feature detection algorithms: A methodology and case study on corner detectors," *IEEE Trans. Imag. Process.*, vol. 12, no. 12, pp. 1668–1676, Dec. 2003.
[28] D. Zhang, L. Fubing, and Y. Le, "An auto-adapted features extraction method based on Harris operator," *Remote Sens. Land Resour.*, vol. 6, no. 2, pp. 35–38, 2006.
[29] Z. Zeng, Z. Jiang, Q. Chen, and P. He, "An improved corner detection algorithm based on Harris," *Adv. Eng. Forum*, vols. 6–7, pp. 717–721, 2012.
[30] K. Sembulingam, *Essentials of Medical Physiology*, 6th ed. New Delhi, India: Jaypee Brothers, 2013.
[31] J. Allen, "Photoplethysmography and its application in clinical physiological measurement," *Physiol. Meas.*, vol. 28, no. 3, pp. R1–R39, Mar. 2007.
[32] J.-X. Wu, C.-M. Li, Y.-R. Ho, M.-J. Wu, P.-T. Huang, and C.-H. Lin, "Bilateral photoplethysmography analysis for peripheral arterial stenosis screening with a fractional-order integrator and info-gap decision-making," *IEEE Sensor J.*, vol. 16, no. 8, pp. 2691–2700, Apr. 2016.
[33] (2019). *NIH Clinical Center*. [Online]. Available: https://Nihcc.app.box.com/v/ChestXray-NIHCC
[34] C.-H. Lin, C.-D. Kan, W.-L. Chen, and P.-T. Huang, "Application of two-dimensional fractional-order convolution and bounding box pixel analysis for rapid screening of pleural effusion," *J. X-Ray Sci. Technol.*, vol. 27, no. 3, pp. 517–535, Jul. 2019.
[35] V. K. Jayasree, T. V. Sandhya, and P. Radhakrishnan, "Non-invasive studies on age related parameters using a blood volume pulse sensor," *Meas. Sci. Rev.*, vol. 8, no. 4, pp. 82–86, 2008.
[36] C.-H. Lin, C.-D. Kan, and W.-L. Chen, "Drainage monitoring system," Taiwan Patent M 565 008, 2018. [Online]. Available: https://twpat2.tipo.gov.tw/tipotwousr/00114/ga-M565008.pdf
[37] *Medical Electrical Equipment—Part 1: General Requirements for Basic Safety and Essential Performance*, Int. Standard IEC 60601-1, 3rd ed., Dec. 2005.
[38] P.-T. Huang, T.-L. Jong, C.-M. Li, W.-L. Chen, and C.-H. Lin, "Integrating flexible sensor and virtual self-organizing DC grid model with cloud computing for blood leakage detection during hemodialysis," *IEEE Trans. Biomed. Circuits Syst.*, vol. 11, no. 4, pp. 784–793, Aug. 2017.

PI-YUN CHEN received the Ph.D. degree from the Graduate School of Engineering Science and Technology, National Yunlin University of Science and Technology, Yunlin, Taiwan, in 2011.

She is currently an Associate Professor with the Department of Electrical Engineering, National Chin-Yi University of Technology, Taichung, Taiwan. She has been the Chief of the Department of Electrical Engineering, National Chin-Yi University of Technology, since 2019. Her current research interests include neural network computing and its applications, fuzzy systems, and advanced control systems.

CHIA-HUNG LIN was born in Kaohsiung, Taiwan, in 1974. He received the B.S. degree in electrical engineering from the Tatung Institute of Technology, Taipei, Taiwan, in 1998, and the M.S. and Ph.D. degrees in electrical engineering from the National Sun Yat-sen University, Kaohsiung, in 2000 and 2004, respectively.

He was a Professor with the Department of Electrical Engineering, Kao-Yuan University, Kaohsiung, from 2004 to 2017. He has been currently a Professor with the Department of Electrical Engineering and a Researcher of Artificial Intelligence Application Research Center, National Chin-Yi University of Technology, Taichung, Taiwan, since 2018. His research interests include neural network computing and its applications, biomedical signal and image processing, healthcare, hemodynamic analysis, and pattern recognition.

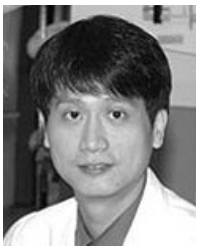

CHUNG-DANN KAN received the M.D. degree from Kaohsiung Medical College, Kaohsiung, Taiwan, in 1993, and the Ph.D. degree from National Cheng Kung University, Tainan, Taiwan, in 2010.

He completed the Residency and Fellowship training in cardiovascular surgery at National Cheng Kung University Hospital, Tainan City, Taiwan. He is currently an Attending Physician with the Department of Surgery, National Cheng Kung University Hospital, and Institute of Clinical and Cardiovascular Research Center, Medical College, Tainan, Taiwan. He has been a Professor with the Department of Surgery, National Cheng Kung University, Tainan, since 2019. His research interests include cardiac regeneration and aortic stent graft.

NENG-SHENG PAI received the B.S. and M.S. degrees from the Department of Automatic Control Engineering, Feng Chia University, Taichung, Taiwan, China, in 1983 and 1986, respectively and the Ph.D. degree from the Department of Electrical Engineering, National Cheng Kung University, Tainan, Taiwan, in December 2002.

He is currently a Professor with the Department of Electrical Engineering, National Chin-Yi University of Technology, Taichung. His current research interests include fuzzy systems, artificial intelligence, imagine processing, advanced control systems, and microprocessor systems. He was the Chairman of the Department, from 2004 to 2007, and was also the Chairman of the Computer Center of the National Chin-Yi University of Technology, from 2013 to 2017.

WEI-LING CHEN was born in Kaohsiung, Taiwan, in 1970. She received the B.S. degree in mechanical engineering from National Cheng Kung University, Tainan, Taiwan, in 1994, and the M. S. and Ph.D. degrees in biomedical engineering from National Cheng Kung University, Tainan, Taiwan, in 1996 and 2015, respectively.

She is currently with the Department of Engineering and Maintenance, Kaohsiung Veterans General Hospital, Kaohsiung, Taiwan, in 2013, and also with the KSVGH Originals and Enterprises, Kaohsiung Veterans General Hospital, Kaohsiung, since 2018. She has also been an Assistant Professor with the Department of Nursing, Mei-Ho University, Pingtung, Taiwan, since 2018. Her research interests include biomedical signal processing, hemodynamic analysis, healthcare, numerical analysis, medical device design, and numerical analysis.

CHIH-HSIEN LI is currently pursuing the B.S. degree with the Department of Electrical Engineering, National Chin-Yi University of Technology, Taichung, Taiwan, since 2017.

His research interests include digital signal processing, embedded system applications, and digital healthcare.